Supplemental Material

for *Core Structure and Non-Abelian Reconnection of Defects in a Biaxial Nematic Spin-2 Bose-Einstein Condensate*

M. O. Borgh and J. Ruostekoski

Mathematical Sciences, University of Southampton, SO17 1BJ, Southampton, United Kingdom

In this Supplemental Material we derive the topologically distinct line defects in the biaxial nematic spin-2 BEC, and discuss experimental preparation of a state with orthogonal, noncommuting vortices. We also provide additional details regarding the ground-state phase diagram, the orientation-dependent instability of a singular vortex with cyclic core, and the construction of a point defect as the termination of a vortex line.

CLASSIFICATION OF VORTICES IN THE BIAXIAL NEMATIC PHASE

Here we formally derive the topologically distinct vortex classes in the BN phase of the spin-2 BEC, using the homotopy theory of defects [1] and following the derivation for liquid crystals [2] and applying the formalism and methods of Ref. [3]. In the atomic spin-2 BEC, the presence of a condensate phase must also be taken into account, and leads to vortices with fractionally quantized superfluid circulation.

A representative BN spinor is

$$\zeta^{\mathrm{BN}} = \frac{1}{\sqrt{2}}\begin{pmatrix}1\\0\\0\\0\\1\end{pmatrix}, \tag{S1}$$

where the spinor components correspond to the spin projection onto the z axis. The biaxial symmetry can most easily be seen by representing the order parameter as a linear combination of spherical harmonics [4] $Z(\theta,\varphi) = \sum_{m=-2}^{+2} Y_{2,m}(\theta,\varphi)\zeta_m$. Inserting ζ^{BN}, we find $Z^{\mathrm{BN}} = \sqrt{15/16\pi}\sin^2\theta\cos(2\varphi)$, shown in Fig. S1.

For the purposes of classifying topological defects, it is easier to work in the Cartesian representation, where the spin-2 order parameter is a symmetric, traceless rank-2 tensor with components [3, 4]:

$$\begin{aligned}
\chi_{xx} &= \frac{\zeta_2+\zeta_{-2}}{\sqrt{2}} - \frac{\zeta_0}{\sqrt{3}},\\
\chi_{yy} &= -\frac{\zeta_2+\zeta_{-2}}{\sqrt{2}} - \frac{\zeta_0}{\sqrt{3}},\\
\chi_{xy} &= i\frac{\zeta_2-\zeta_{-2}}{\sqrt{2}}, \quad \chi_{xz} = -\frac{\zeta_1-\zeta_{-1}}{\sqrt{2}},\\
\chi_{yz} &= -i\frac{\zeta_1+\zeta_{-1}}{\sqrt{2}}, \quad \chi_{zz} = \frac{2}{\sqrt{3}}\zeta_0,
\end{aligned} \tag{S2}$$

where we have used the normalization

$$\frac{1}{2}\mathrm{Tr}(\chi^\dagger\chi) = 1. \tag{S3}$$

For the BN spinor (S1), the tensor order parameter takes the simple form

$$\chi_{\mathrm{BN}} = \begin{pmatrix}1&0&0\\0&-1&0\\0&0&0\end{pmatrix}. \tag{S4}$$

The full set of energetically degenerate BN states can be found by applying SO(3) rotations, represented by orthogonal 3×3 matrices $\mathcal{R}$, and a U(1) phase $e^{i\tau}$. An arbitrary BN order parameter can then be written on the form $\chi = e^{i\tau}\mathcal{R}\chi_{\mathrm{BN}}\mathcal{R}^T$.

The group of transformations formed from all possible combinations of τ and $\mathcal{R}$ is U(1) × SO(3). We now need to find those elements that leave χ_{BN} invariant. It is immediately obvious from Fig. S1, and easily verified, that χ_{BN} is invariant under the identity transformation and the three diagonal SO(3) matrices that correspond to rotations by π around the x, y, and z axes, respectively:

$$\begin{aligned}
\mathbf{1} &= \begin{pmatrix}1&0&0\\0&1&0\\0&0&1\end{pmatrix}, \quad \mathcal{I}_x = \begin{pmatrix}1&0&0\\0&-1&0\\0&0&-1\end{pmatrix},\\
\mathcal{I}_y &= \begin{pmatrix}-1&0&0\\0&1&0\\0&0&-1\end{pmatrix}, \quad \mathcal{I}_z = \begin{pmatrix}-1&0&0\\0&-1&0\\0&0&1\end{pmatrix}.
\end{aligned} \tag{S5}$$

The element

$$\mathcal{C} = \begin{pmatrix}0&1&0\\-1&0&0\\0&0&1\end{pmatrix} \tag{S6}$$

in SO(3) represents the $\pi/2$ counter-clockwise rotation around the z axis, which takes $x \to y$ and $y \to -x$ and thus permutes the nonzero diagonal elements of χ_{BN}. The order parameter is invariant under $\mathcal{C}$ in combination

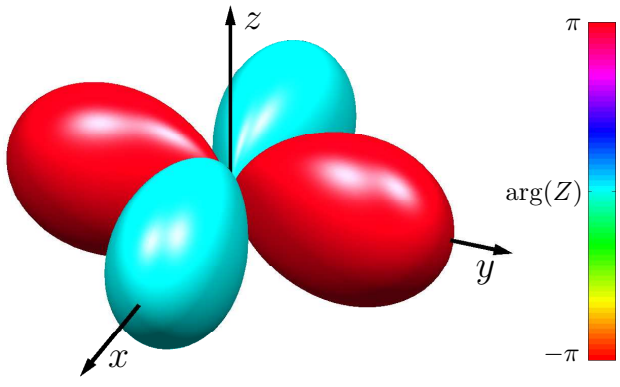

FIG. S1. Spherical-harmonics representation, $Z^{\mathrm{BN}} = \sum_{m=-2}^{+2} Y_{2,m}\zeta_m^{\mathrm{BN}}$, of the representative BN order parameter ζ^{BN} in Eq. (S1). Color represents the complex phase.

with a π rotation of the U(1) phase, $\chi_{\rm BN} = e^{i\pi}\mathcal{C}\chi_{\rm BN}\mathcal{C}^T$. This transformation forms the element $\tilde{\mathcal{C}} = (e^{i\pi}, \mathcal{C})$ in U(1) × SO(3). In the same way, we can construct all remaining transformations that leave $\chi_{\rm BN}$ unchanged as products of $\mathcal{I}_{x,y,z}$ and $\tilde{\mathcal{C}}$ (corresponding to π rotations around $(\hat{\mathbf{x}} \pm \hat{\mathbf{y}})/\sqrt{2}$ and the clockwise rotation by $\pi/2$ around $\hat{\mathbf{z}}$). We conclude that $\chi_{\rm BN}$ is invariant under the eight-element group

$$\tilde{\rm D}_4 = \{\mathbf{1}, \mathcal{I}_x, \mathcal{I}_y, \mathcal{I}_z, \tilde{\mathcal{C}}, \mathcal{I}_x\tilde{\mathcal{C}}, \mathcal{I}_y\tilde{\mathcal{C}}, \mathcal{I}_z\tilde{\mathcal{C}}\}, \tag{S7}$$

formed by the dihedral-4 group $\rm D_4$ in combination with the element $\exp(i\pi) \in$ U(1). Hence the order-parameter space for the BN phase is

$$\mathcal{M} = \frac{\rm U(1) \times SO(3)}{\tilde{\rm D}_4}. \tag{S8}$$

To classify the vortices in the BN phase, we must now find the first homotopy group $\pi_1(\mathcal{M})$. To this end, we find a simply connected covering group by lifting SO(3) to SU(2), using the quaternion representation, where the elements of SU(2) are 2×2 matrices $\mathbf{Q} = e_0\mathbf{1} + i\mathbf{e}\cdot\boldsymbol{\sigma}$, given by four Euler parameters $(e_0, \mathbf{e})$ and the Pauli matrices $\sigma_{x,y,z}$ [5].

As we lift SO(3), the group $\rm D_4$ lifts into the 16-element subgroup $\rm D_4^\star$ of SU(2) according to

$$\begin{aligned} \mathbf{1} &\to \pm\mathbf{1} \\ \mathcal{I}_{x,y,z} &\to \pm i\sigma_{x,y,z} \\ \mathcal{C} &\to \pm\frac{1}{\sqrt{2}}(\mathbf{1} + i\sigma_z) \equiv \pm\sigma, \end{aligned} \tag{S9}$$

and combinations of these. Hence $\tilde{\rm D}_4$ lifts to the 16-element group

$$\tilde{\rm D}_4^\star = \{\pm\mathbf{1}, \pm i\sigma_x, \pm i\sigma_y, \pm i\sigma_z, \pm\tilde{\sigma}, \pm i\sigma_x\tilde{\sigma}, \pm i\sigma_y\tilde{\sigma}, \pm i\sigma_z\tilde{\sigma}\}, \tag{S10}$$

where $\tilde{\sigma}$ includes the $\exp(i\pi)$ phase in analogy with the definition of $\tilde{\mathcal{C}}$. The full subgroup of U(1) × SU(3) that leaves the order parameter invariant is thus

$$\begin{aligned} H = \{&(n, \pm\mathbf{1}), (n, \pm i\sigma_x), (n, \pm i\sigma_y), (n, \pm i\sigma_z), \\ &(n + 1/2, \pm\sigma), (n + 1/2, \pm i\sigma_{x,y,z}\sigma)\}, \end{aligned} \tag{S11}$$

where each element is characterized by an integer n, corresponding to a $2\pi n$ transformation of the U(1) part, and an element of $\tilde{\rm D}_4^\star$, giving 16 elements for each n. Fractional U(1) winding appears when n combines with the U(1) part of $\tilde{\sigma}$. The group composition law is given by $(x, f)(y, g) = (x + y, fg)$. Note that the group is non-Abelian, since in general $fg \neq gf$. It is also a discrete group, and it follows immediately [1] that $\pi_1(\mathcal{M}) = H$.

Topologically distinct vortices correspond to the *conjugacy classes* of $\pi_1(\mathcal{M})$, which, since H is non-Abelian, may contain more than a single element. The conjugacy classes are determined by the SU(2) part of the elements of H. For each $n \in \mathbb{Z}$ we can then directly calculate six conjugacy classes of $\pi_1(\mathcal{M})$:

$$\begin{aligned} &(i) && \{(n, \mathbf{1})\} \\ &(ii) && \{(n, -\mathbf{1})\} \\ &(iii) && \{(n, \pm i\sigma_x), (n, \pm i\sigma_y), (n, \pm i\sigma_z)\} \\ &(iv) && \{(n + 1/2, \sigma), (n + 1/2, -i\sigma_z\sigma)\} \\ &(v) && \{(n + 1/2, -\sigma), (n + 1/2, i\sigma_z\sigma)\} \\ &(vi) && \{(n + 1/2, \pm i\sigma_x\sigma), (n + 1/2, \pm i\sigma_y\sigma)\} \end{aligned} \tag{S12}$$

Recalling the rotations of the BN order parameter corresponding to each element of $\tilde{\rm D}_4^\star$, we then identify the following distinct types of vortices for the case $n = 0$: (i) the trivial element, (ii) singly quantized spin vortex, (iii) half-quantum spin vortex, (iv) half-quantum vortex with $\pi/2$ spin rotation, (v) half-quantum vortex with $3\pi/2$ spin rotation, and (vi) half-quantum vortex with π spin rotation. For $n \neq 0$ we correspondingly get three types of integer vortex, involving 0, 2π and π spin rotations, respectively. In addition we get three types of half-integer vortices with $\pi/2$, $-\pi/2$ and π spin rotations.

VORTEX PREPARATION AND TIME EVOLUTION

Here we consider construction of a wave function representing a pair of noncommuting vortices, and show how such a state could be prepared in experiment. Specifically we construct the wave function of coexisiting $(1/2, \sigma)$ and $(1/2, i\sigma_x\sigma)$ vortices whose reconnection is shown in the main text.

Vortex lines with $(1/2, \sigma)$ and $(1/2, i\sigma_x\sigma)$ charges oriented along the z axis can be separately constructed by applying the corresponding condensate-phase and spin rotations to Eq. (S1) as

$$\zeta^{1/2,\sigma} = e^{i\phi/2}e^{-iF_z\phi/4}\zeta^{\rm BN} = \frac{1}{\sqrt{2}}(1, 0, 0, 0, e^{i\phi})^T \tag{S13}$$

and

$$\begin{aligned} \zeta^{1/2,i\sigma_x\sigma} &= e^{i\phi/2}e^{-i\frac{F_x+F_y}{\sqrt{2}}\frac{\phi}{2}}\zeta^{\rm BN} \\ &= \frac{e^{i\phi/2}}{\sqrt{2}}\begin{pmatrix} \cos\frac{\phi}{2} \\ e^{-i\pi/4}\sin\frac{\phi}{2} \\ 0 \\ -e^{i\pi/4}\sin\frac{\phi}{2} \\ \cos\frac{\phi}{2} \end{pmatrix}, \end{aligned} \tag{S14}$$

respectively, where ϕ is the azimuthal angle. Note how in the latter case, the spin transformation rotates the order parameter about the $(\hat{\mathbf{x}} + \hat{\mathbf{y}})/\sqrt{2}$ as represented in Fig. S1.

To construct wave function simultaneously representing both vortices, we start from Eq. (S13), containing the $(1/2, \sigma)$ vortex, and then add the $(1/2, i\sigma_x\sigma)$ vortex. In this case, however, the order parameter in which the $(1/2, i\sigma_x\sigma)$ is to be added is not spatially uniform. The

axis for the spin rotation corresponding to the $i\sigma_x\sigma$ SU(2) charge is therefore no longer constant, but depends on the position relative to the $(1/2,\sigma)$ vortex. We denote the azimuthal angle around the $(1/2,\sigma)$ vortex by ϕ_1, and choose coordinates such that the new vortex line is some distance away in the $\phi_1=\pi$ direction (for simplicity we first assume the vortex lines to be parallel). Denoting the azimuthal angle relative to the added $(1/2,i\sigma_x\sigma)$ by $\phi_2=0$, we can find the two-vortex wave function as

$$\begin{aligned}\zeta^{\rm pair} &= e^{i\phi_2/2}e^{-i\hat{\mathbf{n}}(\phi_1)\cdot\hat{\mathbf{F}}\phi_2/2}\zeta^{1/2,\sigma}\\ &= \frac{i}{2\sqrt{2}}\begin{pmatrix}(1+e^{i\phi_2})\\ (1-e^{i\phi_2})e^{i\phi_1/4}\\ 0\\ -(1-e^{i\phi_2})e^{3i\phi_1/4}\\ -(1+e^{i\phi_2})e^{i\phi_1}\end{pmatrix}.\end{aligned}\tag{S15}$$

Here $\hat{\mathbf{F}}$ is the vector of spin-2 Pauli matrices. For parallel vortex lines, the solution is exact. However, we are ultimately interested in nonparallel vortex lines that exhibit reconnection. Rotating the direction of the $(1/2,i\sigma_x\sigma)$ vortex line (correspondingly rotating the axis defining ϕ_2), Eq. (S15) becomes approximate, corresponding to a rapidly relaxing excitation. Equation (S15) for perpendicular vortex lines forms the initial state for the non-Abelian reconnection shown in Fig. 2 of the main text.

Vortex lines in the individual components of a spinor BEC can be prepared using Raman transitions [6], where the singular phase profile of the Raman laser is transferred to the condensate. However, Eq. (S15) is not expressed in terms of simple quantized vortex lines in the spinor components and is therefore not directly amenable to imprinting using the Raman process. To find an imprinting scheme, we first note as a general property of the point-group symmetry that the order-parameter rotations that make up a vortex have simplified representations when the spinor is expressed in the basis of spin quantization along the axis of spin rotation. Accordingly applying the corresponding spinor-basis transformation to Eq. (S14), the $(1/2,i\sigma_x\sigma)$ vortex is expressed as

$$\begin{aligned}\tilde{\zeta}^{1/2,i\sigma_x\sigma} &= e^{-i\frac{F_x-F_y}{\sqrt{2}}\frac{\pi}{2}}\zeta^{1/2,i\sigma_x\sigma}\\ &= \frac{1}{\sqrt{2}}\begin{pmatrix}0\\ e^{-3i\pi/4}\\ 0\\ e^{-i\pi/4}e^{i\phi}\\ 0\end{pmatrix}.\end{aligned}\tag{S16}$$

Here, we have introduced $\tilde{\zeta}$ for the spinor represented in the rotated basis. Similarly transforming Eq. (S15), we find that close to $\phi_1=\pi$ it is well approximated by

$$\tilde{\zeta}^{\rm pair}\Big|_{\phi_1\simeq\pi} \simeq \frac{1}{\sqrt{2}}\begin{pmatrix}0\\ e^{-i\pi/4}\\ 0\\ e^{i\pi/4}e^{i\phi_2}\\ 0\end{pmatrix},\tag{S17}$$

exhibiting a singly quantized vortex line only in $\tilde{\zeta}_{-1}$, corresponding to the $(1/2,i\sigma_x\sigma)$ vortex. This suggests a two-step imprinting scheme where first the $(1/2,\sigma)$ vortex is prepared according to Eq. (S13). The effective magnetic field, corresponding to the Zeeman shift, is rotated by $\pi/2$, changing the spinor basis. The $(1/2,i\sigma_x\sigma)$ vortex is then added by additionally preparing a vortex line in $\tilde{\zeta}_{-1}$. This can proceed via population transfer to an intermediate level and then back, using the appropriate laser configuration to imprint the vortex line. In the basis corresponding to the final direction of the magnetic field, the two-vortex wave function is then approximated by the imprinted state

$$\tilde{\zeta}^{\rm pair}\approx\tilde{\zeta}^{\rm imp}=\frac{1}{4\sqrt{2}}\begin{pmatrix}(1+e^{i\phi_1})\\ 2i(-1+e^{i\phi_1})\\ -\sqrt{6}(1+e^{i\phi_1})\\ -2ie^{i\phi_2}(-1+e^{i\phi_1})\\ (1+e^{i\phi_1})\end{pmatrix}.\tag{S18}$$

In regions away from $\phi_1\simeq\pi$ this wave function leaves the BN phase, corresponding to an excitation that relaxes under dissipation. In the two-step protocol, each vortex can be prepared using the Raman process. By imprinting vortex lines along the z axis of the changing spinor basis, perpendicular vortex lines that exhibit non-Abelian reconnection may be prepared.

In order to show the non-Abelian reconnection of vortices with noncommuting charges, we follow the time evolution of the state with two orthogonal vortices described by Eq. (S15). We numerically propagate the coupled Gross-Pitaevskii equations derived from the Hamiltonian density using a split-operator method. In doing so, we include a weak phenomenological dissipation by taking the time $t\to(1-i\eta)t$ [7]. Here we choose $\eta=10^{-3}$.

INTERACTIONS AND STEADY-STATE SOLUTIONS IN THE SPIN-2 BEC

Here we give details of the interaction terms in the Gross-Pitaevskii mean-field Hamiltonian and provide explicit definitions of the steady-state solutions that appear as ground states in addition to the BN in the phase diagram [Fig. 1(a) of the main text] for quadratic Zeeman shift $q<0$. A full derivation of all steady-state solutions of the uniform spin-2 BEC (including those that do not form the ground state for any parameter range) can be found in Ref. [4].

The Hamiltonian density is given by Eq. (1) in the main text. The strengths $c_{0,2,4}$ of the three nonlinear interaction terms are derived from the s-wave scattering lengths $a_{0,2,4}$ that correspond to the three scattering channels of colliding spin-2 atoms, as $c_0=4\pi\hbar^2(3a_4+4a_2)/7m$, $c_2=4\pi\hbar^2(a_4-a_2)/7m$, and $c_4=4\pi\hbar^2(3a_4-10a_2+7a_0)/7m$, where m is the atomic mass. For $q<0$, the BN state forms the ground state of the uniform system when $c_2>c_4/20$ and $c_4<10|q|/n$, where n is the atomic density. This is the case for the most commonly used atoms for spinor-BEC experiments: Measurements in the spin-2 manifold of ^{87}Rb give $a_2-a_0=(3.51\pm0.54)a_B$ and $a_4-a_2=(6.95\pm0.35)a_B$ (where a_B

is the Bohr radius) [8], such that $c_4/c_2 \simeq -0.54$. Also the spin-2 manifold of ^{23}Na is predicted to exhibit the same ground state with $a_0 = 34.9 \pm 1.0$, $a_2 = 45.8 \pm 1.1$, and $a_4 = 64.5 \pm 1.3$ [4], giving $c_4/c_2 \simeq -1.1$.

We now briefly define the remaining steady-state solutions and detail when they form the ground state in the $q < 0$ phase diagram. The spin-2 FM state is the ground state when $c_2 < c_4/20$ for $c_4 < 10|q|/n$, and when $c_2 < |q|/(2n)$ otherwise. The spinor wave function is then $\zeta^{\rm FM} = (e^{i\chi_{+2}}, 0, 0, 0, 0)^T$ [or $\zeta^{\rm FM} = (0, 0, 0, 0, e^{i\chi_{-2}})^T$, which has the same energy for $p = 0$]. In this state, $|\langle\hat{\mathbf{F}}\rangle| = 2$, and the energy per particle is $\epsilon = c_0 n/2 + 2c_2 n + 4q$.

When $c_4 n \geq 10|q|$ and $c_2 > |q|/(2n)$, two additional steady-state solutions appear [4]. The first is

$$\zeta^{\rm C} = \left(e^{i\chi_{+2}}\sqrt{\frac{1+f_z}{3}}, 0, 0, e^{i\chi_{-1}}\sqrt{\frac{2-f_z}{3}}, 0\right)^T \tag{S19}$$

[or $\zeta^{\rm C} = (0, e^{i\chi_{+1}}\sqrt{(2+f_z)/3}, 0, 0, e^{i\chi_{-2}}\sqrt{(1-f_z)/3})^T$], with $|\langle\hat{\mathbf{F}}\rangle| = |f_z| = |q/(c_2 n)|$ and energy $\epsilon = c_0 n/2 + 2q - q^2/(2c_2 n)$. The other is

$$\zeta^{\rm C'} = \left(ie^{i\chi}\frac{\sqrt{1-10q/(c_4 n)}}{2}, 0, \sqrt{\frac{1+10q/(c_4 n)}{2}}, 0, ie^{-i\chi}\frac{\sqrt{1-10q/(c_4 n)}}{2}\right)^T, \tag{S20}$$

with $|\langle\hat{\mathbf{F}}\rangle| = 0$ and energy $\epsilon = c_0 n/2 + 2q - 10q^2/(c_4 n)$. The C (C′) steady-state solution is the ground state when $c_2 < c_4/20$ ($c_2 > c_4/20$). Both spinors continuously approach (different representations of) the cyclic order parameter as $q \to 0^-$.

ORIENTATION-DEPENDENT INSTABILITY OF $(1/2, \sigma)$ VORTEX WITH CYCLIC CORE

Here we study the orientation-dependent instability of the $(1/2, \sigma)$ vortex with the cyclic (β) core that follows from the breakdown of the smooth connection of the different point-group symmetries of the vortex core and the bulk superfluid. The cyclic core breaks axial symmetry as a result of the incommensurate spin symmetries [9], so that its spatial symmetry reflects the threefold discrete spin symmetry of the cyclic order parameter. The left panels of Fig. S2 show the order parameter in the spherical-harmonics representation along with $|A_{30}|$ for the stable vortex with the cyclic (β) core.

The orientation of the BN and cyclic order parameters is fixed by the quadratic Zeeman shift, which corresponds to a magnetic field along the z axis. We have taken this to coincide with the trap rotation axis, but this need not in general be the case. In the middle panel of Fig. S2, the rotation axis has been tilted with respect to the effective field. The vortex-core shape remains robust through a wide range of tilt angles, consistent with the topological origin of the deformation. However, when the tilt angle approaches $\pi/2$, the system can no longer form the continuous connection of the two point-group symmetries, resulting in a destabilization of the vortex structure. The $(1/2, \sigma)$ vortex then gives way to a singly quantized $(1, 0)$ vortex shown in the right-hand panels of Fig. S2. The core of the vortex exhibits a highly complex mixing of cyclic, UN, and BN phases, indicated by $|A_{30}|$ in Fig. S2. At the center of the region, the UN phase appears. This is surrounded by two cyclic and to BN regions, corresponding to the local maxima and minima, respectively.

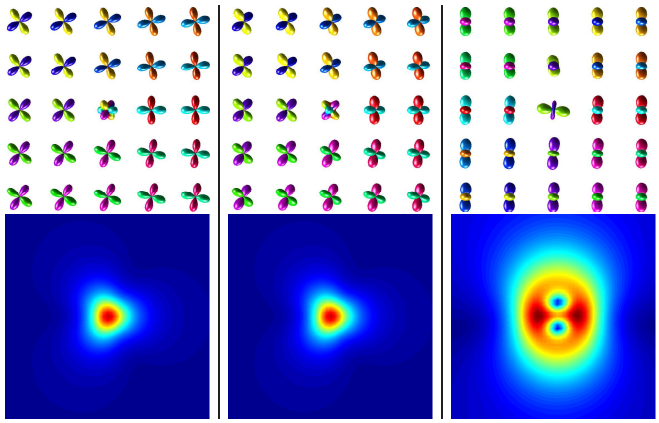

FIG. S2. Relaxed state of an initial $(1/2, \sigma)$ vortex when the quadratic Zeeman shift corresponds to magnetic field making an angle 0 (Left), $\pi/4$ (Middle), and $\pi/2$ (Right) with the trap rotation axis. (Top) Spherical harmonics representation of the relaxed vortex state. (Bottom) $|A_{30}|$ showing the structure and shape of the core. The triangular shape of the cyclic (β) core remains unchanged until a very large angle renders the $(1/2, \sigma)$ vortex unstable, in favor of a singly quantized vortex with a core exhibiting mixing of cyclic, UN and BN phases. $Nc_0 = 5000\hbar\omega\ell^3$, $Nc_2 = -Nc_4 = 1000\hbar\omega\ell^3$, $q = -0.05\hbar\omega$, and $\Omega = 0.17\omega$.

CONSTRUCTION OF POINT DEFECT AS THE TERMINATION OF A VORTEX LINE

In the main text we presented the simplest way of constructing a point-defect texture of the BN order parameter, resulting in an associated spin-vortex line along the z axis. In this construction, one of the principal axes of the BN order parameter (cf. Fig. S1) is aligned with the radius vector. Through a more elaborate construction,

we can avoid the line defect on the positive z axis, illustrated in Fig. 3(c) of the main text. The point defect is still formed by aligning a principal axis with the radius vector. However, by including a local spin rotation about $\hat{\mathbf{r}}$, the BN order parameter can remain nonsingular in the entire upper hemisphere. The point defect then forms the termination point of a spin-vortex line. Energy relaxation in this case leads to the complicated structure of interlocking spin vortex rings shown in Fig. 3(d).

[1] N. D. Mermin, Rev. Mod. Phys. **51**, 591 (1979).

[2] V. Poenaru and G. Toulouse, J. Phys. (Paris) **38**, 887 (1977).

[3] G. W. Semenoff and F. Zhou, Phys. Rev. Lett. **98**, 100401 (2007).

[4] Y. Kawaguchi and M. Ueda, Phys. Rep. **520**, 253 (2012).

[5] H. Goldstein, *Classical Mechanics*, 2nd ed. (Addison Wesley, 1980).

[6] A. Hansen, J. T. Schultz, and N. P. Bigelow, Optica **3**, 355 (2016).

[7] C. W. Gardiner, J. R. Anglin, and T. I. A. Fudge, J. Phys. B: At. Mol. Opt. Phys. **35**, 1555 (2002).

[8] A. Widera, F. Gerbier, S. Fölling, T. Gericke, O. Mandel, and I. Bloch, New J. Phys. **8**, 152 (2006).

[9] M. Kobayashi, Y. Kawaguchi, and M. Ueda, arXiv:0907.3716v2 (2011).